J. Phys.: Condens. Matter **11** (1999) 6395–6411. Printed in the UK PII: S0953-8984(99)03370-6

Pattern formation under bistable electro-optical absorption in quantum wells: I

L L Bonilla†, V A Kochelap†‡ and C A Velasco†§

† Universidad Carlos III de Madrid, Escuela Politécnica Superior, Avenida Universidad 30, E-28911 Leganés, Spain

‡ Department of Theoretical Physics, Institute of Semiconductor Physics, National Academy of Sciences, Kiev 252650, Ukraine

Received 13 April 1999

Abstract. We have formulated and analysed a model of transverse self-sustained pattern formation in a photoexcited and voltage-biased quantum well (QW) structure. Our model explains the formation of patterns of quasi-neutral two-dimensional electron–hole plasma whose intrinsic bistability was shown in recent experiments.

A number of patterns containing regions with different spreading of the electron and hole wave functions and different densities of the two-dimensional electron–hole plasma have been found by using a nonlinear interband light-absorption model. When the transverse extent of the QW layer is large in comparison with the pattern characteristic transverse length scale (of the order of the two-dimensional plasma ambipolar diffusion length), most patterns consist of wide plateaus with high (low) plasma density and relatively narrow domains with low (high) density.

1. Introduction

Recently, electro-optical effects in quantum heterostructures have attracted much attention because of some new unique features of confined electrons [1–7] and numerous device applications based on these effects [8–14]. Among the typical applications of such devices are light modulators, infrared detectors, and other switching devices.

We will focus on the experiments presented in references [1–3] on single- and multiple-quantum-well (QW) GaAs–$Al_xGa_{1-x}As$ heterostructures exposed to an external electric field and to a monochromatic photon source under low-temperature conditions (2–4 K). These experiments revealed interesting phenomena such as bistability, quasi-neutral plasma domains‖, negative differential capacitance and nonlinear screening.

Our aim is to present a model to explain the appearance of quasi-neutral plasma domains in a photoexcited and voltage-biased QW (vertical dimension $\approx$ 100–200 Å). Preliminary results were reported in [15], and in [16], where they were explained in terms of a quantum-confined Stark effect in these structures. The geometry of the problem consists of a single GaAs QW of width $2d$ subject to a constant electric field due to uniformly distributed charges of a parallel-plate capacitor. The distance between the capacitor plates is $2d_c$, such that $d \ll d_c$, and the field is parallel to the direction of vertical growth of the sample. Furthermore, a uniform monochromatic photon source photoexcites the QW (see figure 1). Investigating the red-shift

§ Author to whom any correspondence should be addressed.

‖ Although in the cited references, the term 'charge-density domains' is used to describe the quasi-neutral two-dimensional electron–hole plasma, we prefer the term 'quasi-neutral plasma domain' or 'plasma domain.'

0953-8984/99/336395+17$30.00

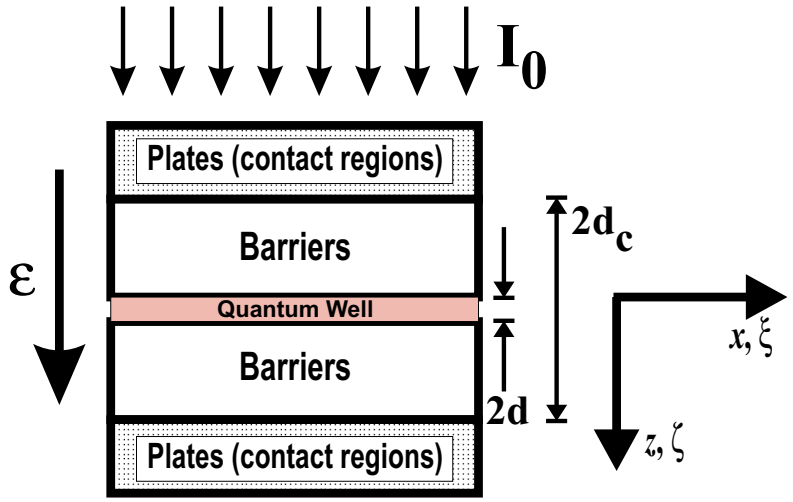

Figure 1. The geometry under consideration. We show a single QW layer of width $2d$ and the capacitor plates (contact regions), to which an external voltage is applied. The sample is exposed to a uniform illumination I_0. The electric field is in the vertical (z-axis) direction.

of Raman scattering data, the simultaneous existence of two sets of coupled plasmon modes was noticed. This indicates the formation of plasma domains with different electron–hole concentrations (see [1–3], and references therein). This is a single-well phenomenon, and differs from resonant tunnelling [17–20]. However, similar bistable phenomena were found in reference [21] for an InAlAs/InGaAs superlattice embedded in a p–i–n structure.

Our approach is based upon consideration of the widely separated characteristic length scales which are involved in the problem. There are six important length scales: the screening length of the two-dimensional (2D) electron–hole gas (l_{sc}, related to the semiconductor properties and Poisson's equation; reference [22] shows that $l_{sc} \sim a^*$, the effective Bohr radius), the well width ($2d$), the characteristic transverse electron wavelength (λ_{dB}, the de Broglie wavelength in the transverse direction), the ambipolar diffusion length ($L_{\mathcal{D}} = \sqrt{\mathcal{D}\tau_R}$, which is the characteristic length scale of the transverse patterns; $\mathcal{D}$ is the ambipolar diffusion coefficient and τ_R is the recombination time), the well transverse dimension (L_x), and the distance between the capacitor plates ($2d_c$). For a typical experiment with a GaAs sample, the following relations hold: $L_x \gg d_c > L_{\mathcal{D}} \gg \lambda_{dB}, d, l_{sc}$ (for example: $L_x \approx 100$–$200\ \mu$m; $2d_c \approx 0.5$–$1\ \mu$m [23]; $L_{\mathcal{D}} \approx 0.2$–$0.5\ \mu$m; $\lambda_{dB} \approx 600$ Å; $2d \approx 200$ Å; $l_{sc} \approx 100$ Å). The inequality $d_c > L_{\mathcal{D}} \gg d$ allows us to neglect nonuniformities in the electric charge induced on the capacitor plates by the patterns, as will be shown in section 3.4. Thus it can be assumed that the external electric field is uniformly applied throughout the sample. The motions in the vertical and transverse directions are uncoupled because the ratio $\theta = d/L_{\mathcal{D}}$ is very small and $L_{\mathcal{D}}$ is much larger than λ_{dB} and l_{sc}. Motion in the vertical direction is quantized ($\lambda_{dB} \sim d$), and we can find the discrete energy levels as functions of the electron and hole concentrations by using the Hartree approximation in the coupled Schrödinger–Poisson system [22]. We can analyse the electron–hole relaxation and transverse transfer by means of semiclassical drift–diffusion equations [14, 24–27]. An important simplification is the 'quasi-neutrality' of the system, which follows from $\theta^2 \ll 1$.

Our analysis indicates that there may be different patterns in the QW transverse direction when the electro-optical absorption process is in its bistable regime. The patterns consist

of high- and low-plasma-concentration domains (corresponding to weak and strong electro-absorption respectively), separated by transition regions of widths of the order of $L_{\mathcal{D}}$.

The results of our work are presented in two papers. This paper introduces the basic equations of the model and the main simplifications imposed to study the resulting problem. We include as well the analysis of the bistable regimes in homogeneous 2D plasma, and the possible patterns for QWs with infinite transverse extensions. In the second paper we will show how these patterns can be controlled by the boundary conditions in the transverse direction, and will analyse their stability and dynamical behaviour. Thus the conditions for experimental detection of the patterns can be established.

2. Model and basic equations

Let us consider a heterostructure with a single QW layer of thickness $2d$. Define a coordinate system with the x- and y-axes lying in the plane of the layer, and the z-axis perpendicular to it (see figure 1). The transverse dimensions are L_x and L_y, much larger than d. We apply to the QW a constant electric field ($\mathcal{E}$) due to uniformly distributed charges of a parallel-plate capacitor in the z-direction, and a transversely uniform monochromatic photon source. As mentioned in the introduction, there is no influence of the patterns in the charge distribution of the capacitor plates. This assumption will be justified later.

Since the transverse nonuniformities are very smooth in comparison with the thickness $2d$ and the de Broglie wavelengths of the electrons and holes, we can concentrate on the wave functions and energies corresponding to the quantization of the carriers in the well. The transverse electron motion is assumed to be entirely classical. We assume that the effective masses of electrons and holes, are equal† and the QW is infinitely deep. The latter is assumed to simplify our calculations, and can be justified by considering that our typical ground-state energies are of the order of 10 meV (see table A1 in the appendix and figure 2), whereas the barrier height is 300–400 meV [28]. Then, the Schrödinger equation in the Hartree approximation [22] and its boundary conditions take the form

$$\begin{aligned}
&-\frac{\hbar^2}{2m}\Delta_3\Psi_{e,h}(x,y,z) \mp (V(x,y,z) - e\mathcal{E}z)\Psi_{e,h}(x,y,z) = E_{e,h}\Psi_{e,h}(x,y,z)\\
&\int_{-d}^{d} \mathrm{d}z \ \left|\Psi_{e,h}(x,y,z)\right|^2 = 1\\
&\Psi_{e,h}(x,y,z=\pm d) = 0
\end{aligned} \tag{1}$$

where '$-$' ('+') corresponds to electrons (holes), E_e (E_h) is the electron (hole) subband energy, and $V = e\Phi$ ($e > 0$), Φ being the Hartree potential originating from the electron–hole plasma. We anticipate that the leading-order approximation to $\Psi_{e,h}$ will be independent of the transverse coordinates x, y due to the assumed large aspect ratios $L_{x,y}/d$. Then the normalization condition is such that $|\Psi_{e,h}|^2$ is a linear probability density. V is a function of the transverse coordinates; thus the leading-order approximations to $\Psi_{e,h}$ and $E_{e,h}$ depend parametrically on them.

The Hartree potential Φ obeys the three-dimensional Poisson equation, and therefore V can be expressed as

$$\Delta_3 V = \frac{e^2}{\epsilon_0}(\mathcal{N}\,|\Psi_e|^2 - \mathcal{P}\,|\Psi_h|^2) \tag{2}$$

† The analysis of the system with different effective masses leads to results which are not qualitatively different from those presented here.

where ϵ_0 is the dielectric constant of the material and $\mathcal{N}$ ($\mathcal{P}$) is the two-dimensional density of electrons (holes). We have assumed that only the lowest e and h subbands are populated. This approximation is easily seen to be justified by studying the excited energy levels of electrons and holes when compared to their Fermi level. As boundary conditions for (2), we require that V is constant far away from the well layer.

For the transverse redistribution of electrons and holes, we use the drift–diffusion equations [14, 24–27]:

$$\frac{\partial \mathcal{N}}{\partial t} + \boldsymbol{\nabla}_2 \cdot \boldsymbol{\mathcal{J}}_n = \mathcal{G} - \mathcal{R} \tag{3}$$

$$\frac{\partial \mathcal{P}}{\partial t} + \boldsymbol{\nabla}_2 \cdot \boldsymbol{\mathcal{J}}_p = \mathcal{G} - \mathcal{R}. \tag{4}$$

Here $\boldsymbol{\mathcal{J}}_n$ and $\boldsymbol{\mathcal{J}}_p$ are two-dimensional fluxes for both types of carrier:

$$\boldsymbol{\mathcal{J}}_n = -\mu_n \mathcal{N}\left(-\frac{1}{e}\boldsymbol{\mathcal{F}}_n\right) - \mathcal{D}_n \boldsymbol{\nabla}_2 \mathcal{N} \tag{5}$$

$$\boldsymbol{\mathcal{J}}_p = \mu_p \mathcal{P}\left(\frac{1}{e}\boldsymbol{\mathcal{F}}_p\right) - \mathcal{D}_p \boldsymbol{\nabla}_2 \mathcal{P} \tag{6}$$

where $\mu_{n,p}$ and $\mathcal{D}_{n,p}$ are the mobility and diffusion coefficients, $\boldsymbol{\nabla}_2 = \boldsymbol{i}\,\partial/\partial x + \boldsymbol{j}\,\partial/\partial y$, and $\boldsymbol{\mathcal{F}}_{n,p}$ are the forces acting on the two-dimensional electrons and holes, respectively. $\mathcal{G}$ and $\mathcal{R}$ are the rates of photogeneration and recombination (both will be specified later).

Regarding the forces $\boldsymbol{\mathcal{F}}_{n,p}$, we should recall that the concepts of two-dimensional electrons and holes are introduced because the electrostatic potential is a smooth function of the transverse coordinates. Then the energies of the two-dimensional subbands are functions of these coordinates (in our case $E_e(x, y)$, $E_h(x, y)$), and to leading order we can neglect the intersubband transitions induced by the potentials. Thus the quasi-classical transverse motion of the carriers occurs in a potential landscape given by $E_{e,h}(x, y)$. Once the latter are known, the forces acting on the carriers are [14]

$$\boldsymbol{\mathcal{F}}_n = -\boldsymbol{\nabla}_2 E_e \qquad \boldsymbol{\mathcal{F}}_p = -\boldsymbol{\nabla}_2 E_h. \tag{7}$$

Equations (3) and (4) should be supplemented with appropriate boundary conditions at the edges of the QW layer. In particular, we can set the total transverse current to zero:

$$e(\boldsymbol{\mathcal{J}}_p - \boldsymbol{\mathcal{J}}_n)_{\text{norm}} = 0 \tag{8}$$

and suppose that at the edges there is a finite rate of electron–hole recombination:

$$(\boldsymbol{\mathcal{J}}_n)_{\text{norm}} = \mathcal{S}N \tag{9}$$

where $(\boldsymbol{\mathcal{J}}_n)_{\text{norm}}$ means the component of the electron flux perpendicular to the edges. $\mathcal{S} \geqslant 0$ is the 'edge recombination velocity'†.

Table 1 and table 2 present the dimensionless variables and parameters which we will use to transform our equations to dimensionless form. Note that in the following, we will use that the inverse aspect ratio θ is a small parameter (see table A1 in the appendix):

$$\theta \ll 1. \tag{10}$$

† $\mathcal{S}$ is entirely analogous to the surface velocity of recombination, which is used to describe electron–hole recombination near interfaces of bulk-like semiconductors. In interfaces of bulk semiconductors, $\mathcal{S}$ is generally dependent on the position in the edge. In our case, it will be constant. These boundary conditions are relevant for the second paper of this work.

Table 1. Dimensionless variables.

Variable	Dimensionless form	Constant
Electric field	$q = \dfrac{\mathcal{E}}{\mathcal{E}_0}$	$\mathcal{E}_0 = \dfrac{E_0}{ed}$
Electron and hole subband energies	$\epsilon_{e,h} = \dfrac{E_{e,h}}{E_0}$	$E_0 = \dfrac{\hbar^2}{2md^2}$
Electron and hole 2D concentrations	$n = \dfrac{\mathcal{N}}{\mathcal{N}_0}$, $p = \dfrac{\mathcal{P}}{\mathcal{N}_0}$	$\mathcal{N}_0 = \dfrac{\epsilon_0 E_0}{e^2 d}$
Electron and hole wave functions	$\psi_{e,h} = \sqrt{d}\,\Psi_{e,h}$	
Hartree potential energy	$v = \dfrac{V}{E_0}$	
Light intensity	$i = \dfrac{I_\omega}{I_0}$	$I_0 = \dfrac{\epsilon_0 E_0 \overline{h}\omega}{e^2 d \tau_R A_0}$
Time	$\tau = \dfrac{t}{\tau_R}$	
Transverse well dimension	$L = \dfrac{L_x}{L_\mathcal{D}}$ [a]	
x-coordinate	$\xi = \dfrac{x}{L_\mathcal{D}}$ [a]	
y-coordinate	$\eta = \dfrac{y}{L_\mathcal{D}}$ [a]	
z-coordinate	$\zeta = \dfrac{z}{d}$	

[a] $L_\mathcal{D}$ is defined in the body of the text ($L_\mathcal{D} = \sqrt{\mathcal{D}_0 \tau_R}$, with $\mathcal{D}_0 = [2\beta/(1+\beta)]E_0\mu_n/e$), and represents the length scale of the patterns in the transverse direction of the QW. The latter will be represented by a vector $\boldsymbol{r}$ whose components are the transverse coordinates in dimensionless form, i.e. $\boldsymbol{r} \equiv (\xi, \eta)$.

Table 2. Dimensionless parameters.

Parameter
$\theta = \dfrac{d}{L_\mathcal{D}}$
$\beta = \mu_p/\mu_n$
$\lambda = \dfrac{\pi\epsilon_0\overline{h}^2}{me^2d}$
$\gamma = \dfrac{\mu_0 E_0 \tau_R}{eL_\mathcal{D}^2}$ [a]

[a] μ_0 represents the reference mobility defined in section 2.2.

2.1. Simplification and solution of the Schrödinger–Poisson system

In dimensionless form, the Schrödinger and Poisson equations (1) and (2) may be written as follows (see table 1):

$$\left(\frac{\partial^2}{\partial\zeta^2} + \theta^2\Delta_2 + \epsilon_{e,h} \pm v(\zeta;\boldsymbol{r},\tau) \mp q\zeta\right)\psi_{e,h}(\zeta;\boldsymbol{r},\tau) = 0 \tag{11}$$

$$\left(\frac{\partial^2}{\partial\zeta^2} + \theta^2\Delta_2\right)v(\zeta;\boldsymbol{r},\tau) = \frac{n(\boldsymbol{r},\tau)+p(\boldsymbol{r},\tau)}{2}(|\psi_e(\zeta;\boldsymbol{r},\tau)|^2 - |\psi_h(\zeta;\boldsymbol{r},\tau)|^2) + \frac{n(\boldsymbol{r},\tau)-p(\boldsymbol{r},\tau)}{2}(|\psi_e(\zeta;\boldsymbol{r},\tau)|^2 + |\psi_h(\zeta;\boldsymbol{r},\tau)|^2). \tag{12}$$

Here Δ_2 is the two-dimensional Laplacian. The wave functions are adiabatical functions of $\boldsymbol{r}$ and τ because the potential is a functional of the electron and hole densities.

We obtain the important quasi-neutrality relation between n and p by integrating (12) with respect to ζ and using (i) the normalization conditions for $\psi_{e,h}$, and (ii) the boundary condition that the potential is a constant far from the QW (we assume smoothness of the solutions to our problem):

$$n(\boldsymbol{r},\tau) - p(\boldsymbol{r},\tau) = \mathrm{O}(\theta^2) \tag{13}$$

as $\theta \to 0$†. The leading-order approximations to equations (11) and (12) obey the system

$$\left(\frac{\partial^2}{\partial\zeta^2} + \epsilon_{e,h} \pm v(\zeta;n) \mp q\zeta\right)\psi_{e,h}(\zeta;n) = 0 \tag{14}$$

$$\frac{\partial^2}{\partial\zeta^2}v(\zeta;n) = n(|\psi_e(\zeta;n)|^2 - |\psi_h(\zeta;n)|^2) \tag{15}$$

to be solved with the boundary and normalization conditions previously discussed. Notice that the wave functions, the energies $\epsilon_{e,h}$, and the Hartree potential depend on the transverse coordinates and time through their dependence on the electron density $n(\boldsymbol{r},\tau)$ inside the QW layer. Our leading-order approximation yields the same equations for the Schrödinger–Poisson problem as in the one-dimensional theory of [3]. However, the quasi-neutrality of the electron–hole plasma is derived in our theory (rather than assumed), which moreover describes the transverse plasma motion (see details below).

The approximate system (14) and (15) possesses the following symmetry properties:

$$v(\zeta;n) = -v(-\zeta;n) \qquad \psi_e(\zeta;n) = \psi_h(-\zeta;n). \tag{16}$$

Thus, to leading-order approximation, the Hartree potential v is

$$v(\zeta;n) = v_0(\zeta;n) + \phi(\boldsymbol{r},\tau) + \mathrm{O}(\theta) \qquad -1 < \zeta < 1 \tag{17}$$

$$v_0(\zeta;n) = n\int_{-1}^{1} \mathrm{d}\zeta'\, \mathcal{K}(\zeta,\zeta')\left|\psi_e(\zeta';n)\right|^2 \tag{18}$$

where

$$\mathcal{K}(\zeta,\zeta') \equiv \frac{1}{2}(|\zeta-\zeta'| - |\zeta+\zeta'|).$$

Here $n(\boldsymbol{r},\tau)$ and $\phi(\boldsymbol{r},\tau)$ are as-yet unknown functions independent of ζ which will be determined later.

The Hartree potential (17) and the symmetry properties (16) allow us to find $\psi_{e,h}$ by solving the following single Schrödinger equation:

$$\frac{\mathrm{d}^2\psi}{\mathrm{d}\zeta^2} + (\epsilon + v_0 - q\zeta)\psi = 0 \tag{19}$$

where

$$\psi(\pm 1) = 0 \qquad \int_{-1}^{1} |\psi(\zeta;n)|^2\ \mathrm{d}\zeta = 1.$$

We obtain for electrons and holes $\psi_e = \psi(\zeta;n)$, $\psi_h = \psi(-\zeta;n)$, respectively. The eigenvalue ϵ depends parametrically on $n(\boldsymbol{r},\tau)$ and we have

$$\epsilon_e(\boldsymbol{r},\tau) = -\phi(\boldsymbol{r},\tau) + \epsilon(n(\boldsymbol{r},\tau)) \qquad \epsilon_h(\boldsymbol{r},\tau) = \phi(\boldsymbol{r},\tau) + \epsilon(n(\boldsymbol{r},\tau)). \tag{20}$$

Equation (19) is the same as equation (3) of reference [3]. However, equation (20) shows that there is a difference $2\phi(\boldsymbol{r},\tau)$ between the energies of holes and electrons corresponding

† This fact will allow us to use plasma and electron concentrations as equivalent terms for the rest of the paper.

to an additional Hartree potential drop due to the transverse carrier motion. This potential drop depends on the transverse patterns of the plasma and it will be calculated later.

The solutions of equation (19) were found by means of a variational method. We introduced a functional $\mathcal{H}\{\psi\}$, corresponding to equation (19), and used as trial functions a set of orthogonal polynomials in the interval $[-1, 1]$. Figure 2 depicts the energy ϵ as a function of the plasma density n for different values of the electric field q. The increase in the electron and hole energies with carrier concentration arises, obviously, from the screening of the applied field.

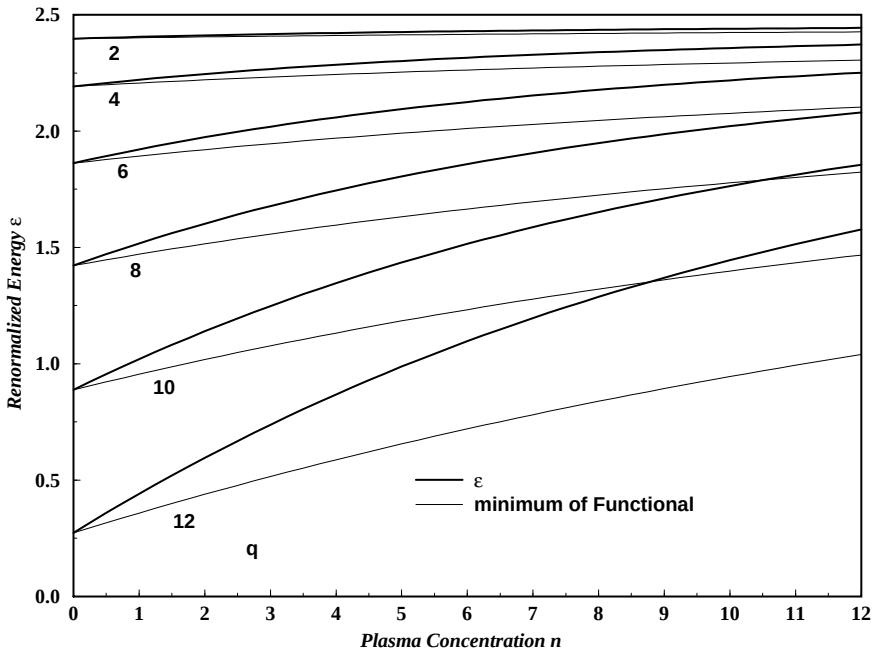

Figure 2. The dependence of the renormalized energy ϵ on the plasma concentration at different dimensionless electric fields ($q = 2, \ldots, 12$). The minimum of the functional $\mathcal{H}\{\psi\}$, used to calculate ϵ, is shown as well.

2.2. Transverse transfer and relaxation of photoexcited carriers

We now determine the second contribution to the Hartree potential, ϕ, and the electron density, n, from the drift–diffusion equations (3) and (4) written in dimensionless form as

$$\frac{\partial n}{\partial \tau} + \gamma \nabla_r \cdot \left\{ \frac{\mu_n}{\mu_0} [n \nabla_r (\phi - \epsilon(n)) - \alpha(n) \nabla_r n] \right\} = \frac{\mathcal{G} - \mathcal{R}}{\mathcal{N}_0/\tau_R} \tag{21}$$

$$\frac{\partial p}{\partial \tau} - \gamma \nabla_r \cdot \left\{ \frac{\mu_p}{\mu_0} [p \nabla_r (\phi + \epsilon(n)) + \alpha(n) \nabla_r p] \right\} = \frac{\mathcal{G} - \mathcal{R}}{\mathcal{N}_0/\tau_R}. \tag{22}$$

In these equations, carriers move on the plane due to the forces (7), which can be calculated using the energies (20). Note that the potentials v_0 and ϕ generate the forces acting on the electrons and holes in different ways. The potential v_0 generates equal forces for both types of carrier through the dependence $\epsilon(n)$, whilst the potential $\phi(\boldsymbol{r})$ generates oppositely directed

forces:

$$\mathcal{F}_e = -\frac{E_0}{L_\mathcal{D}}\,\boldsymbol{\nabla}_r(\epsilon(n)-\phi) \qquad \mathcal{F}_p = -\frac{E_0}{L_\mathcal{D}}\,\boldsymbol{\nabla}_r(\epsilon(n)+\phi) \tag{23}$$

which lead to the separation of the carriers in the plane layer.

In equations (21) and (22), we have defined the function $\alpha(n) = e\mathcal{D}_{n,p}/E_0\mu_{n,p}$, which does not depend on the type of the carriers (n or p) and can be easily found from the Einstein relation.

The charge continuity equation is obtained by subtracting (22) from (21). Inserting the quasi-neutrality condition (13) in the result we find

$$\boldsymbol{\nabla}_r \cdot \left\{ \frac{\mu_n}{\mu_0}[(1+\beta)n\,\boldsymbol{\nabla}_r\phi - (1-\beta)(n\,\boldsymbol{\nabla}_r\epsilon + \alpha(n)\,\boldsymbol{\nabla}_r n)] \right\} = 0. \tag{24}$$

Equation (24) can be integrated once with the help of (8), thereby providing the following equation for $\phi(\boldsymbol{r},\tau)$:

$$\boldsymbol{\nabla}_r\phi = \frac{1-\beta}{1+\beta}\left(\alpha(n) + n\frac{\partial\epsilon(n)}{\partial n}\right)\frac{1}{n}\,\boldsymbol{\nabla}_r n. \tag{25}$$

Equation (25) can be readily solved:

$$\phi(n) = \frac{1-\beta}{1+\beta}\left(\int^n \frac{\alpha(n)\,\mathrm{d}n}{n} + \epsilon(n)\right) + \text{constant}. \tag{26}$$

Thus once $n(\boldsymbol{r},\tau)$ is known, we can calculate the electrostatic potential in the QW, $v(\zeta; n)$.

To write down explicitly the equation for n, we shall specify the generation and recombination rates as

$$\mathcal{G} = A(n,q,\omega)\frac{I_\omega}{\hbar\omega} \qquad \mathcal{R} = \frac{\mathcal{N}}{\tau_R} \tag{27}$$

where I_ω is the intensity of the incident light (constant, i.e. independent of the transverse coordinates), A is the absorption factor, dependent on n and q throughout the energy spectrum of the carriers, and τ_R is the recombination time, which is assumed to be independent of n. To obtain the final nonlinear equation for n, we must add the drift–diffusion equations (21) and (22), use the quasi-neutrality condition (13), and define the reference mobility

$$\mu_0 = \frac{2\mu_n\mu_p}{\mu_n+\mu_p} = \frac{2\beta}{1+\beta}\mu_n.$$

The result is

$$\frac{\partial n}{\partial\tau} - \boldsymbol{\nabla}_r\cdot\{\mathcal{D}(n,q)\,\boldsymbol{\nabla}_r n\} = a(n,q,\omega)i - n \equiv R(n,q,\omega,i) \tag{28}$$

where the dimensionless light intensity i is defined in table 1 and we have used the notation $a = A/A_0$ (A_0 is the maximum absorption). In (28) we have defined a 'diffusion-like' coefficient $\mathcal{D}$, a function of the plasma concentration n and the electric field q, as

$$\mathcal{D}(n,q) \equiv \alpha(n) + n\frac{\partial\epsilon(n,q)}{\partial n}. \tag{29}$$

It is important to notice that the diffusion coefficient $\mathcal{D}(n,q)$ is strictly positive for all $n \geqslant 0$. In fact, it can be shown that $\alpha(n) > 0$, whereas figure 2 shows that the energy ϵ is an increasing function of n.

The characteristic length defined by (28) is

$$L_\mathcal{D} = \sqrt{\mathcal{D}_0\tau_R} \qquad \text{with } \mathcal{D}_0 = \frac{2\beta}{1+\beta}\frac{E_0\mu_n}{e}$$

(the latter coincides with the diffusivity of a degenerate plasma with Fermi energy equal to E_0). With this definition, $\gamma = 1$ in equations (21) and (22), which is why γ does not appear in equation (28).

Let us restrict consideration to patterns which depend on a single transverse coordinate, let us say ξ. Then (28) leads to

$$\frac{\partial n}{\partial \tau} - \frac{\partial}{\partial \xi}\left\{\mathcal{D}(n,q)\frac{\partial n}{\partial \xi}\right\} = a(n,q,\omega)i - n \equiv R(n,q,\omega,i). \tag{30}$$

Equation (30) reduces to the rate equation model used in reference [3] for coordinate-independent electron densities. The boundary condition (9) is transformed into

$$j_n = -\mathcal{D}(n,q)\frac{\partial n}{\partial \xi} = \pm s^{(\pm)} n \tag{31}$$

where $s = \mathcal{S}L_{\mathcal{D}}/\mathcal{D}$, and the signs $\pm$ correspond to the right and left edges of the QW layer:

$$\xi^{(\pm)} = \pm\frac{L_x/2}{L_{\mathcal{D}}} = \pm\frac{1}{2}L.$$

2.3. Model of absorption

Generally, the bistable regimes arise if the absorption factor $A(n, q, \omega)$ is a superlinear function of the plasma concentration and the right-hand side of equation (30) has several solutions at fixed q. Several of our results do not require specification of $A(n)$, but for our numerical results we follow papers [1–3] and suppose that the absorption is due to the generation of excitons, i.e., the bound and continuum states of electron–hole pairs. The Coulomb attraction between an electron and a hole leads to a hydrogen-like resonance spectrum below the band-gap energy. These excitons are associated with the two-dimensional electron and hole subbands. A fast exchange between the excitons and the electron–hole states is supposed; thus we can characterize the system by the electron and hole concentrations. In the case of deep QWs and a large exciton radius, the exciton energy E_{ex} follows the positions of the electron and hole subbands. Let E_g be the optical band gap in the QW material; then the resonant absorption corresponds to the energy $E_g + E_n + E_p - E_{ex}$ and depends on the carrier concentration through $E_{n,p}$. Assuming a Lorentz shape of the absorption factor as a function of the photon energy $\hbar\omega$, we can write

$$A(n,q,\omega) = A_0 a(n,q,\omega) \qquad a(n,q,\omega) = \frac{\Lambda^2}{(\epsilon(n,q) - \Delta)^2 + \Lambda^2} \tag{32}$$

where $\Delta = -(E_g - E_{ex} - \hbar\omega)/2E_0$ is the detuning of the photon energy, and Λ is the dimensionless bandwidth of the exciton in units of $2E_0$. The exciton bandwidth is typically in the range of a few meV. It is obvious that for the shape of the absorption (32) the right-hand side of equation (30) can have more than one solution at a detuning $\Delta(\omega) > \epsilon(0, q)$. With this formula for the absorption we complete the model and the basic equations for the patterns.

3. Analysis of stationary patterns

The analysis of stationary patterns will be focused on one-dimensional patterns. We will find the singular points of the stationary equation of (30), we will study the behaviour of the solutions near those points, and we will consider the patterns that appear for transversely infinite samples.

Notice also that the following analysis will consider several parameters of our problem as fixed constants: the electric field q, the frequency of emission of photons ω, the light detuning

$\Delta(\omega)$, and the temperature T. Thus the main variable is the plasma concentration n that will depend on the light intensity i and the transverse coordinate ξ. The influence of the sample transverse dimensions L and the edge recombination rates $s^{\pm}$ will be studied in the second paper of this work.

3.1. Stationary patterns and singular points

The steady solutions of equation (30) solve a second-order nonlinear parabolic differential equation with mixed boundary conditions, which may be solved by phase plane methods (see related studies in references [29, 30]). This equation is

$$-\frac{\mathrm{d}}{\mathrm{d}\xi}\left\{\mathcal{D}(n)\frac{\mathrm{d}n}{\mathrm{d}\xi}\right\} = R(n,i)$$

or

$$\frac{\mathrm{d}}{\mathrm{d}n}\left\{\frac{1}{2}\mathcal{D}^2(n)k^2(n)\right\} = -\mathcal{D}(n)R(n,i) \equiv \Gamma(n,i) \tag{33}$$

where $k \equiv \mathrm{d}n/\mathrm{d}\xi$. The singular points of equations (33) are given by the algebraic equation

$$R(n^*;i) = 0 \tag{34}$$

which will give one, two or three solutions depending upon the value of the light intensity i. Figure 3 depicts the solutions of the equation. Notice the existence of two critical light intensity values (i_l and i_h) where the generation and recombination rates are tangent. These values delimit the range of bistability (i_l, i_h). In this interval, there exist three solutions of

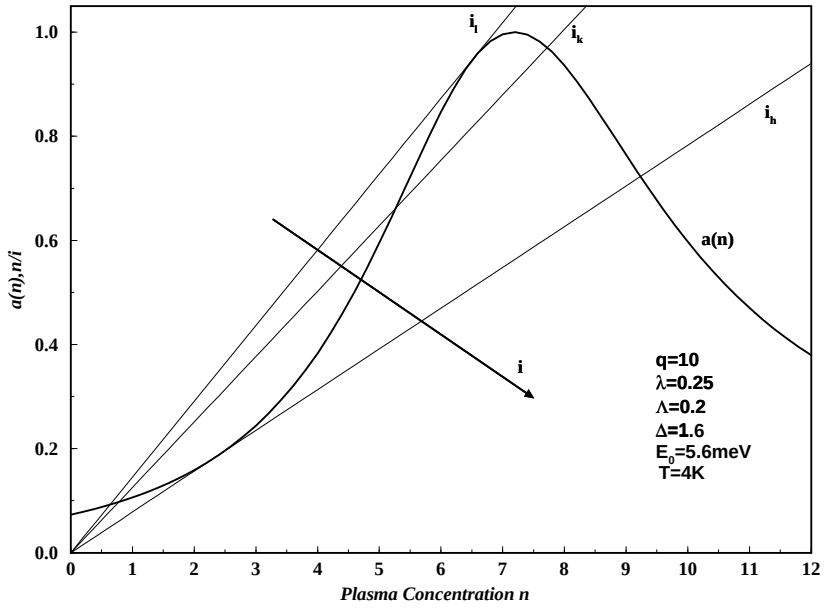

Figure 3. Bistability regions at fixed electric field. The plots show the dimensionless generation and recombination rates by depicting the absorption coefficient a (Lorentzian curve), and the ratio n/i (straight lines whose slope decreases when the light intensity increases). It is clear that there exist two light intensity values i_l and i_h where both curves are tangent and (34) has two solutions. In the range (i_l, i_h), there are three solutions of (34) and bistability occurs. The critical value i_k is explained in the text and the parameter values are written down in the body of the figure.

equation (34), which we will denote as $n^* = n_1, n_2, n_3$. The character of these singular points is different, and will determine the bistable behaviour of the patterns.

3.1.1. Behaviour near singular points. When $|n - n^*| \ll 1$, we can use the approximation $\Gamma(n) \approx \Gamma'(n^*)(n - n^*)$, where

$$\Gamma'(n^*) = -\left\{\mathcal{D}'(n^*)R(n^*) + \mathcal{D}(n^*)R'(n^*)\right\} = -\mathcal{D}(n^*)R'(n^*). \tag{35}$$

Thus, we obtain

$$\frac{\mathrm{d}}{\mathrm{d}n}\left\{\frac{1}{2}\mathcal{D}^2(n)k^2(n)\right\} = -\mathcal{D}(n^*)R'(n^*)(n - n^*) \tag{36}$$

and integrating:

$$\mathcal{D}^2(n)k^2(n) = -\mathcal{D}(n^*)R'(n^*)(n - n^*)^2. \tag{37}$$

It is easily seen from figure 3 that n_1 and n_3 are saddle points ($R'(n^*) < 0$), and n_2 is a centre ($R'(n^*) > 0$). When $n^* = n_1, n_3$, we obtain from equation (37) the behaviour of the solution near saddle points:

$$k(n) \approx \pm\frac{\sqrt{\mathcal{D}(n^*)|R'(n^*)|}}{\mathcal{D}(n)}(n - n^*) \qquad |n - n^*| \ll 1. \tag{38}$$

However, in the case where $n^* = n_2$, we must linearize equations (33), obtaining

$$-\mathcal{D}(n_2)\frac{\mathrm{d}^2 n}{\mathrm{d}\xi^2} = R'(n_2)(n - n_2) \qquad |n - n_2| \ll 1$$

$$\frac{\mathrm{d}^2 n}{\mathrm{d}\xi^2} + \frac{R'(n_2)}{\mathcal{D}(n_2)}(n - n_2) = 0$$

$$\frac{\mathrm{d}^2 n}{\mathrm{d}\xi^2} + \Omega^2(n - n_2) = 0. \tag{39}$$

The solution of this equation is

$$n - n_2 = a_0 \sin(\Omega\xi + \varphi) \qquad \text{where } \Omega = \sqrt{R'(n_2)/\mathcal{D}(n_2)}.$$

And the resulting minimum period is

$$\xi_p^{\min} = 2\pi\sqrt{\frac{\mathcal{D}(n_2)}{R'(n_2)}}. \tag{40}$$

3.1.2. Critical intensity and phase portraits. A first integral of the stationary equations (33) is

$$\frac{1}{2}\mathcal{D}^2(n)\left(\frac{\mathrm{d}n}{\mathrm{d}\xi}\right)^2 + U(n, i) = C_1 \qquad \text{where } U(n, i) = \int_{n_1}^{n} \mathrm{d}n'\ R(n', i)\mathcal{D}(n'). \tag{41}$$

Then the solutions are implicitly given by

$$\pm\int^{n} \frac{\mathcal{D}(n')\ \mathrm{d}n'}{\sqrt{2(C_1 - U(n'))}} = \xi + C_2 \tag{42}$$

where C_1 and C_2 are constants.

There exists a critical value for which there are two heteroclinic orbits connecting the two saddle points. This value is easily obtained from equation (41), via the equality

$$U(n_3(i_k), i_k) = 0. \tag{43}$$

This equation is clearly a modified 'equal-area rule' [31, 32]. i_k divides the interval $[i_l, i_h]$ (on which $n(i)$ is multivalued) into two subintervals, $[i_l, i_k)$ and $(i_k, i_h]$. On each subinterval the phase portrait is similar: one of the saddles has a homoclinic orbit enclosing the centre. When $i \in (i_l, i_k)$, the homoclinic orbit belongs to $(n_3, 0)$, whereas it belongs to $(n_1, 0)$ when $i \in (i_k, i_h)$. Figure 4 depicts these phase portraits for some typical intensity values ($i_l < i < i_k$ (a), $i = i_k$ (b), and $i_k < i < i_h$ (c)) together with the singular points of (34).

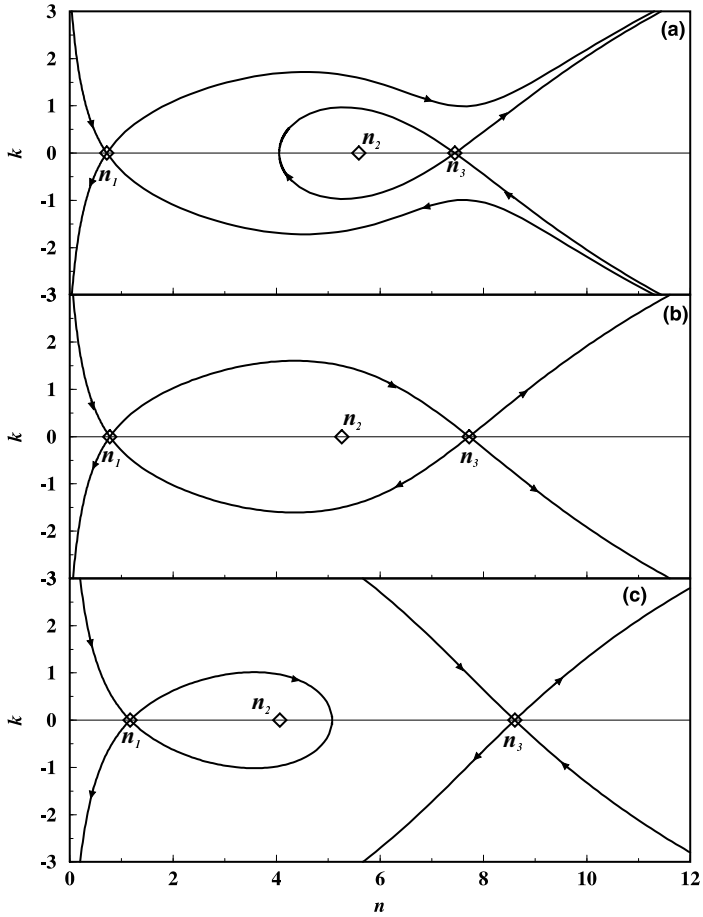

Figure 4. Phase portraits for $i_l < i < i_k$ (a), $i = i_k$ (b), and $i_k < i < i_h$ (c). The curves depicted are the separatrices; no other trajectories are portrayed. Diamonds represent the singular points $(n_1, 0)$, $(n_2, 0)$, and $(n_3, 0)$.

3.2. Transverse patterns for infinite QWs

The solutions of the boundary value problem may be easily visualized by means of the phase portrait analysis. Let us study the case with $L = \infty$. Bounded solutions for all ξ correspond to homoclinic, heteroclinic, or closed orbits. Closed orbits correspond to periodic plasma densities $n(\xi)$. When $i \in (i_l, i_k)$ ($i \in (i_k, i_h)$), the solution corresponding to the homoclinic orbit represents a domain of depleted (high) plasma concentration on a medium of high (low) density (see figure 5(a) and figure 5(c), respectively). For the special case $i = i_k$ the heteroclinic

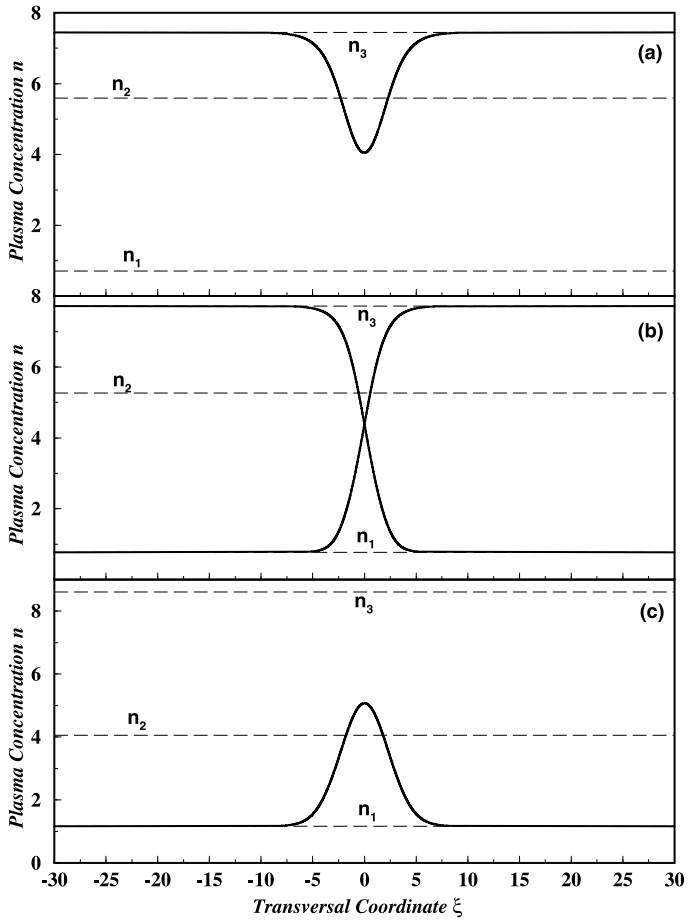

Figure 5. Three basic types of pattern for infinite dimension of the QW layer. (a) corresponds to the interval $[i_l, i_k)$, (b) corresponds to $i = i_k$, and (c) corresponds to the interval $(i_k, i_h]$.

orbits connecting the two saddles represent coexistence of spatially separated low- and high-density plasmas. Two symmetric patterns are possible as shown in figure 5(b) ('kink-like' patterns).

3.3. Radially symmetric patterns

It is interesting to notice that we found also patterns with radial symmetry. These patterns arise as a result of expressing (28) in polar coordinates with its radially symmetric form:

$$\frac{\partial n}{\partial \tau} - \frac{1}{r}\frac{\partial}{\partial r}\left\{ r\mathcal{D}(n,q)\frac{\partial n}{\partial r}\right\} = R(n,q,\omega,i) \tag{44}$$

where r is the radial coordinate.

In this case we found similar structures to those of figure 5. Figure 6 presents two of those solutions for $i_l < i < i_k$ (a), and $i_k < i < i_h$ (b). Both curves represent radial anti-soliton and soliton patterns: (a) is a low-absorption spot in a high-absorption environment, and (b) is a high-absorption spot in a low-absorption environment.

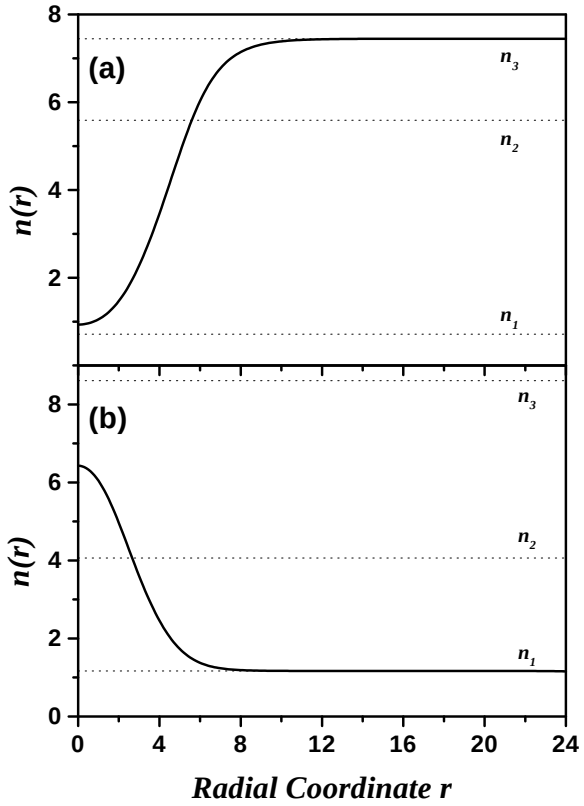

Figure 6. Radially symmetric stationary patterns for $i_l < i < i_k$ (a) and $i_k < i < i_h$ (b). Both cases present patterns in the form of radial anti-soliton and soliton. n_1, n_2, and n_3 represent the solutions of equation (34).

Notice that we have presented and discussed the patterns in terms of redistribution of the plasma over the QW layer. The above results can be used to find the wave function spreading across the well [16] and the three-dimensional configuration of the electrostatic potential between the capacitor plates.

3.4. The configuration of the external electrostatic potential

The potential distribution outside the QW is a solution of the Laplace equation (there is no net charge density outside) in the two strips of the plane (ξ, Z), $Z = \theta\zeta$, limited by both capacitor plates and both QW edges. The electrostatic potential between the capacitor plates and the corresponding QW edge can be calculated analytically [33]. It is a functional of the potential (17) induced by a pattern. The numerical evaluation of the electrostatic potential yields figure 7 for the pattern distribution of figure 5(a) (we have subtracted the contribution of the external field for the sake of clarity). Notice that the potential distribution due to the pattern has a value of a few millivolts at distances of the order of $L_{\mathcal{D}}$, and vanishes when $Z > L_{\mathcal{D}}$. We verified and confirmed our assumption about the uniform distribution of the electric field throughout the QW because the disturbance of the external potential originating from the plasma redistribution within the QW disappears in distances of the order of $L_{\mathcal{D}}$, and this disturbance is negligible when compared to the potential due to the capacitor plates.

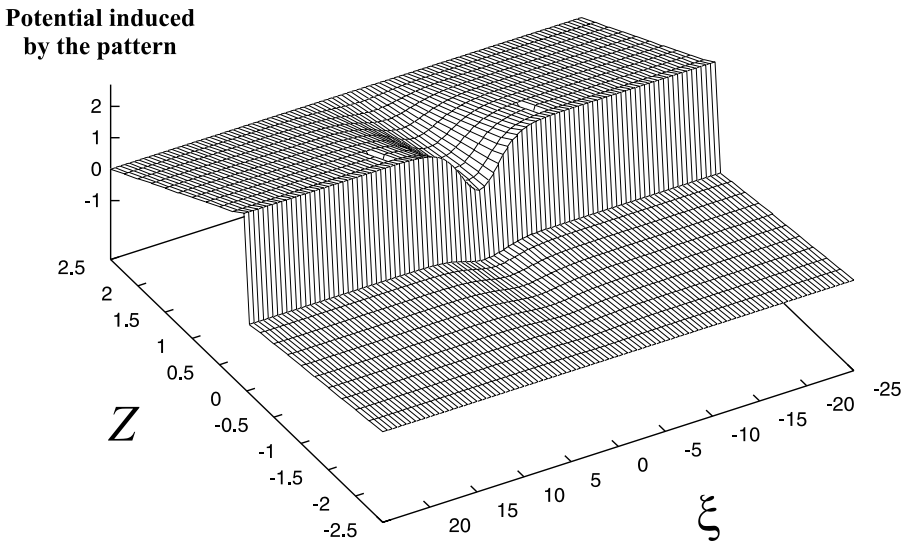

Figure 7. The dimensionless potential distribution outside the QW due to the pattern configuration of figure 5(a), where we have not included the contribution of the external electric field. The distance between the plates is 1 μm. Notice the step-like jump in the potential at the positions $Z \equiv \theta\zeta = \pm\theta$, which correspond to the QW edges; thus on the Z-scale, the QW has almost negligible width.

4. Conclusions

The bistable behaviour of electro-optical effects may appear in different heterostructures in diverse electrical and optical regimes: photoexcited QW structures in an external electric field [1–3], superlattices embedded in p–n junctions [21] (for both cases, vertical current is not needed), self-electro-optical effect devices [8–14] (where the external circuit controls the effect), etc. In fact, all these structures are layered systems with local feedback in which bistability should induce formation of transverse patterns.

In this first part of our study we have formulated and analysed a model of pattern formation in a GaAs QW heterostructure under bistable electro-optical absorption. The model includes: self-consistent calculations of the wave functions and subband energies of the photoexcited electrons and holes in an strongly biased QW, nonlinear interband light absorption, the configuration of the electrostatic potential, its screening, and the transverse motion of the two-dimensional electron–hole plasma. The vertical and transverse motions of the carriers are *strongly coupled* due to the electrostatic interaction. However, the separation in the scales of transverse and vertical effects (see section 1) allowed us to consider them separately to leading-order approximation, and to establish the quasi-neutrality of the electron–hole plasma. A consequence of the carrier-density dependence of the subband energies is the unexpectedly large renormalization of the diffusion coefficient (through the density-dependent forces appearing in the ambipolar drift–diffusion equation) in the resulting boundary value problem (30) and (31). The transverse redistribution of the carriers induces the electrostatic potential, and adiabatically drives the electron and hole wave functions, and the subband energies.

The second part of our work will present a more detailed discussion of the results for patterns in QWs of finite transverse dimension and their stability.

Acknowledgments

We thank Dr V N Sokolov for useful discussions. We are indebted to the Dirección General de Enseñanza Superior (Spanish Ministry of Education) for sabbatical support (VAK) and for financial support through grant PB97-0088, and to the UE Training and Mobility of Researchers Programme through contract ERBFMBXCT970157. One of us (CAV) acknowledges the support of the Fundación General de la Universidad Carlos III de Madrid.

Appendix. Dimensionless variables and constants

In this appendix we are going to give some numerical values for a GaAs QW layer (see references [1–3, 24]). For a GaAs QW structure, the following values are typically chosen for the variables involved in our analysis: $m = 0.068m_0$, $\epsilon_0 = 13.1\epsilon_v$, $\mu_n = 8500$ cm^2 V^{-1} s^{-1}, and $\mu_p = 400$ cm^2 V^{-1} s^{-1}; here m_0 is the electron rest mass ($m_0 = 9.109 \times 10^{-31}$ kg), and ϵ_v the dielectric constant of vacuum ($\epsilon_v = 8.85 \times 10^{-12}$ C V^{-1} m^{-1}). Considering a QW of width $2d = 200$ Å, a maximum absorption $A_0 = 0.05$, a value of $\overline{h}\omega = 1.9$ eV, and a recombination time $\tau_R = 10^{-10}$ s, we obtain the numerical results shown in table A1.

Table A1. Typical numerical values of normalizing constants.

Parameter	Value
E_0 (meV)	5.6
$\mathcal{E}_0$ (kV cm^{-1})	5.6
$\mathcal{N}_0$ (cm^{-2})	4×10^{10}
$\mathcal{D}_0$ (cm^2 s^{-1})	4.5
$L_{\mathcal{D}}$ (μm)	0.2
$I_0/\overline{h}\omega$ (photons cm^{-2} s^{-1})	8.1×10^{21}
I_0 (kW cm^{-2})	2.4
λ_{dB} (Å)[a]	630
a^* (Å) (effective Bohr radius)[b]	100
θ	0.05
β	0.05
λ	0.25

[a] $\lambda_{dB} = 2\pi\overline{h}/\sqrt{2mE_0}$; see [22].
[b] $a^* = 4\pi\epsilon_0\overline{h}^2/(me^2)$; see [22].

References

[1] Merlin R 1989 *Spectroscopy of Semiconductor Microstructures (NATO ASI Series B: Physics, vol 206)* (Dordrecht: Kluwer) p 347
[2] Merlin R, Mestres N, McKiernan A, Oh J and Bhattacharya P K 1990 *Surf. Sci.* **228** 88
[3] Merlin R and Kessler D A 1990 *Phys. Rev.* B **41** 9953
[4] Haug H 1988 *Optical Nonlinearities and Instabilities in Semiconductors* (New York: Academic)
[5] Bastard G, Mendez E E, Chang L L and Esaki L 1983 *Phys. Rev.* B **28** 3241
[6] Schmitt-Rink S, Chemla D S and Miller D A B 1989 *Adv. Phys.* **38** 89
[7] Chemla D S 1993 *Phys. Today* (June) 46
[8] Saleh B E A and Teich M C 1991 *Fundamentals of Photonics* (New York: Wiley)

[9] Miller D A B, Chemla D S, Damen T C, Wood T H, Burrus C A, Gossard A C and Wiegmann W 1984 *Appl. Phys. Lett.* **45** 13
[10] Miller D A B, Chemla D S, Damen T C, Wood T H, Burrus C A, Gossard A C and Wiegmann W 1985 *IEEE J. Quantum Electron.* **21** 1462
[11] Lentine A L, Hinton H S, Miller D A B, Henry J E, Cunningham J E and Chirovski L M F 1989 *IEEE J. Quantum Electron.* **25** 1928
[12] Miller D A B 1990 *Opt. Quantum Electron.* **22** S-61
[13] Abe Y and Tokuda Y 1993 *Appl. Phys. Lett.* **63** 3259
[14] Mitin V V, Kochelap V A and Stroscio M A 1999 *Quantum Heterostructures for Microelectronics and Optoelectronics* (New York: Cambridge University Press)
[15] Bonilla L L, Kochelap V A, Sokolov V N and Velasco C A 1997 *Phys. Status Solidi* b **204** 559
[16] Bonilla L L, Kochelap V A, Sokolov V N and Velasco C A 1998 *J. Phys. C: Solid State Phys.* **31** L539
[17] Esaki L and Chang L L 1974 *Phys. Rev. Lett.* **33** 495
[18] Bonilla L L, Galán J, Cuesta J A, Martínez F C and Molera J M 1994 *Phys. Rev.* B **50** 8644
[19] Bonilla L L 1995 *Nonlinear Dynamics and Pattern Formation in Semiconductor and Devices* ed F J Niedernostheide (Berlin: Springer)
[20] Aguado R, Platero G, Moscoso M and Bonilla L L 1997 *Phys. Rev.* B **55** R16 053
[21] Couturier J, Voisin P and Harmand J C 1993 *J. Physique Coll.* **3** C5 253
Couturier J, Voisin P and Harmand J C 1994 *Appl. Phys. Lett.* **64** 742
Couturier J, Voisin P and Harmand J C 1995 *Semicond. Sci. Technol.* **10** 881
[22] See, e.g., Ando T, Fowler A B and Stern F 1982 *Rev. Mod. Phys.* **54** 437 and references therein
[23] Merlin R 1997 private communication
[24] Sze S M 1981 *Physics of Semiconductor Devices* 2nd edn (New York: Wiley)
Sze S M 1985 *Semiconductor Devices, Physics and Technology* (New York: Wiley)
[25] Reggiani L (ed) 1985 *Hot-Electron Transport in Semiconductors* (Berlin: Springer)
[26] Markowich P A, Ringhofer C and Schmeiser C 1990 *Semiconductor Equations* (Vienna: Springer)
[27] Shaw M P, Mitin V V, Schöll E and Grubin H L 1992 *The Physics of Instabilities in Solid State Electron Devices* (New York: Plenum)
[28] Roßmanith M, Leo J and von Klitzing K 1990 *Proc. 22nd Int. Conf. on the Physics of Semiconductors (Thessaloniki)*
[29] Kochelap V A and Sokolov V N 1971 *Ukr. Phys. J.* **16** 1082
[30] Bonilla L L and Higuera F J 1991 *Physica* D **52** 458
[31] Butcher P N 1967 *Rep. Prog. Phys.* **30** 97
[32] Schöll E 1987 *Nonequilibrium Phase Transitions in Semiconductors* (New York: Springer)
[33] Kellog O D 1953 *Foundations of Potential Theory* (New York: Dover)